Journal of The Electrochemical Society, **155** (12) G274-G282 (2008)
0013-4651/2008/155(12)/G274/9/$23.00 © The Electrochemical Society

Models of Ionic Transport for Silicon-Glass Anodic Bonding

M. Fabbri[z] **and J. R. Senna***

Instituto Nacional de Pesquisas Espaciais, Laboratorio Associado de Materiais e Sensores, Sao Jose dos Campos, Sao Paulo 12227-010, Brazil

We solve numerically the coupled Poisson and transport equations for the motion of ions within the glass during anodic bonding in order to obtain the external current vs time curves and the charge density profiles within the sodium-depleted zone. We consider two simple models for the mobile ions. In both, the sodium cations are assumed to be the most mobile species. In one model the only additional mobile species are anions of the same initial concentration. They represent the compensating nonbridging oxygens. The only free parameter is the relative mobility of anions and cations. In the other model we assume the presence of additional cations and anions which could model the presence of dissociated water in a leached layer. The best agreement with experimental current vs time curves is obtained with the second model, but only if the initial concentration of dissociated water is close to the initial concentration of sodium in the glass. Redistribution of H^+ ions in the "leached layer" model is essential in lowering the local electric field within the bulk sodium-depleted zone. There are significant differences in the final charge density profiles obtained from both models, and the ones in the second one are more consistent with recent measurements in the literature.
 [DOI: 10.1149/1.2988127]

Manuscript submitted April 18, 2008; revised manuscript received August 27, 2008. Published October 9, 2008.

Since it was introduced in 1969 by Wallis and Pomerantz,[1] anodic bonding has become a routine technique for glass sealing of microelectromechanical devices. A simple assembly depicted in Fig. 1 is usually employed, where a high voltage difference V_0 (~600 to 1000 V) is applied to the glass-silicon (Si-g) pair, which is heated to around 300°C. The polarity must be as shown: silicon at the anode, glass as the cathode. At those temperatures, sodium ions in the glass have appreciable mobility and drift toward the cathode. The sodium drift causes a charged depletion layer near the Si-g interface, with very high local electric field, which brings the interfaces in close contact. Meanwhile, oxygen anions from the sodium-depleted region migrate toward the anode. After half a minute or so, a strong, clear, and homogeneous silicon oxide bond layer is developed at the Si-g interface.[1,2]

Current applied research in anodic bonding aims at processes that could be carried out at lower temperatures and lower external potentials, thus allowing safe anodic encapsulation of delicate devices. A detailed understanding of the bonding mechanism requires a correct account of the ionic processes within the sodium-depleted region of the glass. It is already well established that bonding is triggered mainly by sodium drift toward the cathode; issues still remain, however, as to which is the actual source of the oxygen which forms the bonding oxide at the anode. The more traditional models assume that the nonbridging oxygens (NBOs), which were attached to the sodium network modifiers in the glass, become available to migrate toward the anode from the sodium-depleted region.[3] However, detailed analysis by Nitzsche et al.[4] using in situ elastic recoil detection (ERDA) and NMR spectrum of the bulk glass suggests that there are not any NBOs in sodium-borosilicate glasses commonly used for anodic bonding. Also, hydrogen H^+ drift was found to take place in the sodium-depleted zone.[4] They therefore attributed oxygen migration toward the anode to OH^- anions originating from water dissociation within the glass surface "leached" layer.

Our purpose here is to investigate both the NBO and the "leached-layer" pictures with a detailed microscopic ionic transport model. We first state the basic balance and constitutive equations for the more relevant ion species, under reasonable approximations supported by what is already established experimentally (see, e.g., the recent review of Knowles and van Helvoort[5]). The detailed ionic transport within the sodium-depleted layer is likely to have a direct influence on the behavior of the external electric current during the bonding process. However, a correct account of the relationship between the ion fluxes in the glass and the observed external electric current seems to have been overlooked in the anodic bonding literature. We give a simplified but correct treatment which is suitable for the microscopic transport model adopted here.

We have succeeded only in solving the transport equations numerically. That is because of (*i*) the strong dependence of the ionic conductivity on the local ionic charge and (*ii*) the presence of distinct mobile ionic species within the depletion zone. We have to deal with many equations which do not combine in simple forms. Instead of trying to reduce the number of equations, we chose to adopt a simple and intuitive numerical procedure which closely follows the actual ionic transport at each time interval.

We have found it useful to relate the numerical solutions to the analytic Albaugh model,[6] where only sodium cation displacement is considered. His results are also quickly recovered as a particular case from the microscopic ohmic transport equations. The detailed measurements of Albaugh[6] are employed here as a reference for the numerical solutions because they were taken with deposited metallic electrodes, thus minimizing the effect of surface contact enlargement that usually occurs with point electrodes, and within a heat reservoir.

We close by showing that the numerical simulations account well for the observed electric transient during bonding. They support simple thermal-activated ionic transport within the depleted layer. The role of hydrogen H^+ redistribution in the leached layer is also investigated. The numerical solutions show that in the leached-layer picture, the observed external current behavior is only reproduced when there is a close balance between the sodium content in the glass and the ionic densities of the drifting H^+–OH^- pairs.

Charge Displacement within the Glass

In this section we state all the basic equations for the charge distribution and transport within the depleted zone. The numerical procedure used to solve them is described below. We assume blocking electrodes, that is, the anode and the cathode do not supply ions to the bulk glass. We also assume the ionic species arriving from the glass are totally consumed and charge neutralized as they arrive at the electrodes. Actually, sodium can crystallize at the cathode,[7] and oxygen from the glass builds the oxide layer bonding at the silicon

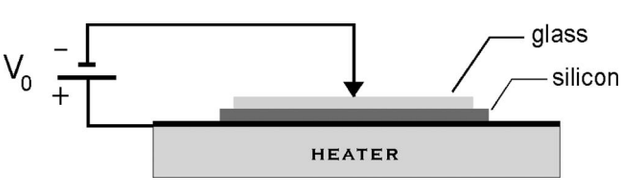

Figure 1. Basic apparatus for glass to silicon anodic bonding.

* Electrochemical Society Active Member.
[z] E-mail: fabbri@las.inpe.br

interface. Both of these layers, which are neglected here, can cause an additional potential drop, reducing the effective electric field within the glass.

We consider a one-dimensional model where ionic transport is restricted to a fixed direction x. The external field is applied along the x direction, with the anode at $x = 0$ and the cathode at $x = L$ (L being the glass thickness).

Experimental findings strongly suggest that the ionic transport is thermally activated and carrier diffusion is small[4] at the time scale relevant for the bonding process. We therefore adopt simple ohmic laws, coupled to advective fluxes, to model the charge transport.

Initially, the sodium mobile ions (of local uniform charge density ρ_0) are attached to an immobile background of negative ions of uniform charge density $-\rho_0$. Under the influence of an external potential V_0, we assume that the uniform cloud of cations Na^+ moves as a whole toward the negative electrode with a mobility μ_{Na^+}. Because there is no source of sodium ions at the anode, the resulting sodium spatial charge distribution is a stepwise profile

$$\rho_{Na^+}(x,t) = \rho_0\theta(x - \Gamma) \quad [1]$$

where $\Gamma = \Gamma(t)$ is the depletion layer (DL) front and $\theta(x)$ is the usual unit step function (1 for $x \geqslant 0$ and 0 for $x < 0$). The displacement of $\Gamma(t)$ is given by the local sodium flux J_{Na}

$$\rho_0\frac{d\Gamma}{dt} = J_{Na}(\Gamma) \quad [2]$$

A variety of distinct constitutive models can be considered for the ionic flux; the simple ohmic dependence here adopted is

$$J_{Na} = \sigma_{Na^+}E = \mu_{Na^+}\rho_{Na^+}E \quad [3]$$

where σ_{Na^+} is the sodium conductivity of the glass sample.

As the DL develops under the influence of an external potential V_0, anions (possibly O_2^-, O^-, or OH^-) and cations (possibly H^+ or other less-mobile glass components) are released to move within the sodium-free region, $0 < x < \Gamma$. We take into account only the most representative anion and cation species. Labeling $-\rho_-(x,t)$ the mobile anion charge and $\rho_+(x,t)$ the mobile cation charge, the total local charge is

$$\rho(x,t) = -\rho_0 - \rho_-(x,t) + \rho_+(x,t), \quad \text{for } 0 < x < \Gamma \quad [4]$$

The region outside the DL is always charge neutral, and therefore the electric field E is uniform at all times in the region $\Gamma < x < L$. Within the DL, the field E must comply with the Gauss–Poisson equation

$$\frac{\partial E}{\partial x} = \rho/\varepsilon \quad [5]$$

where ε is the local dielectric constant.

For a given total external potential V_0, E must be normalized by the condition

$$V_0 = \int_0^L E dx \quad [6]$$

The mobile ions inside the DL satisfy continuity equations

$$\frac{\partial \rho_-}{\partial t} = -\frac{\partial J_-}{\partial x} \quad [7]$$

$$\frac{\partial \rho_+}{\partial t} = -\frac{\partial J_+}{\partial x} \quad [8]$$

Finally, constitutive equations for the ion fluxes must be specified. For the simple ohmic transport, we have

$$J_- = -\sigma_- E \quad [9]$$

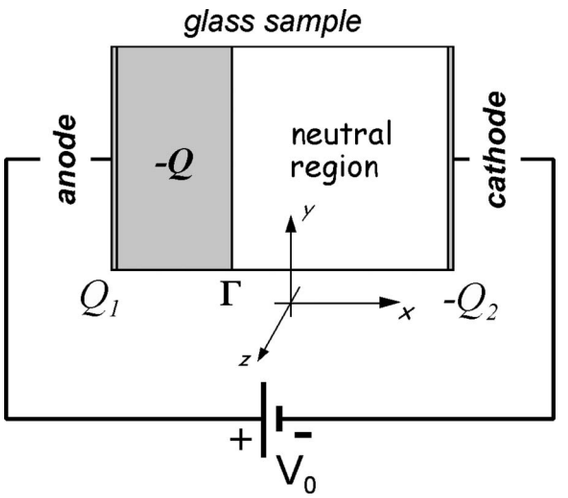

Figure 2. Basic electric scheme (not to scale) of the anodic bonding setup.

$$J_+ = \sigma_+ E \quad [10]$$

where the ionic conductivities are given by the local charges and mobilities

$$\sigma_+ = \mu_+\rho_+ \quad [11]$$

$$\sigma_- = \mu_-\rho_- \quad [12]$$

We assume positive values for vector quantities pointing in the positive x direction, and the symbols for charges and charge densities always stand for their absolute values.

Equations 2-12 are a nonlinear set of strongly coupled equations, which are solved here in the general case by an iterative, moving boundary finite-difference technique.

The External Electric Current

Usually, the bonding process is monitored by recording the time dependence of the current through the high-voltage source. In order to relate the external current to the ion fluxes inside the sample, we apply Gauss law and the superposition principle to obtain the relative contributions to the net local electric field at regions near the electrodes. Unfortunately, there is no simple relationship linking the ionic fluxes to the external current. We develop here a convenient form that must be evaluated from the detailed solutions for the local electric field inside the glass sample.

We assume blocking electrodes, i.e., only electrons are able to charge the metallic electrodes on both sides of the bonding sample. Inside the glass, only ionic currents are allowed (no free electrons). Cations are consumed at the cathode in reactions involving the electrons injected from the external circuit, and the anions react with the anode, forming the bonding oxide and feeding electrons to the external circuit.

At any time, consider the simplified scheme depicted in Fig. 2, where $Q_1(t)$ is the electric charge at the metallic anode electrode, $-Q_2(t)$ the electric charge at the metallic cathode electrode, and $-Q(t)$ the total charge at the DL.

Within the one-dimensional approximation, the electric field E inside the glass ($0 < x < L$) depends only on x. The metallic anode and cathode resemble infinite uniform charged planes, while in the depleted region $0 < x < \Gamma$ the total charge $Q(t)$ has a density profile $\rho(x,t)$. The field E near the electrodes, inside the glass, is the sum of the electric field due to the charged electrodes (E^1) and the field produced by the charged layer (E^2), and is obtained by a straightforward application of Gauss law and superposition. Consider as a Gaussian surface a rectangular box enclosing the glass

region, with left wall at $x = 0_+$ and right wall at $x = L_-$, each with area S. The analysis follows the usual plane capacitor model with infinite plate approximation. We have

$$E^1(0_+) = E^1(L_-) = \frac{Q_1 + Q_2}{2\varepsilon S} \quad E^2(0_+) = \frac{Q}{2\varepsilon S} \quad E^2(L_-) = \frac{-Q}{2\varepsilon S}$$

and therefore

$$E(0_+) = \frac{Q_1 + Q_2 + Q}{2\varepsilon S} \quad E(L_-) = \frac{Q_1 + Q_2 - Q}{2\varepsilon S} \qquad [13]$$

The detailed profile of $E(x)$ for $0 < x < \Gamma$ is strongly dependent on the local distribution of Q inside the DL.

During a time interval Δt, electronic charges are transferred to the metallic electrodes from the external circuit and from the electrodes to the ions that arrive from the glass. The charge transfer from the voltage source V_0 must be symmetric. If Δq is the electronic charge that arrives at the anode from the external source, then it must also deliver a charge amount of $-\Delta q$ to the cathode. Coming from the glass, during the same time interval, charge quantities of ΔQ^C and $-\Delta Q^A$ arrive at the cathode and the anode, respectively. Thus

$$Q_1(t + \Delta t) = Q_1(t) + \Delta q - \Delta Q^A$$

$$-Q_2(t + \Delta t) = -Q_2(t) - \Delta q + \Delta Q^C$$

$$-Q(t + \Delta t) = -Q(t) - \Delta Q^C + \Delta Q^A$$

Inserting those values in Eq. 13, we obtain in the limit $\Delta t \to 0$

$$\begin{cases} \varepsilon \dfrac{dE(0_+)}{dt} = J_{ext} - J_{anions} \\ \varepsilon \dfrac{dE(L_-)}{dt} = J_{ext} - J_{cations} \end{cases} \qquad [14]$$

The current through the high-voltage source is $i = SJ_{ext}$, S being the front surface area of the glass. Equation 14 relates the external current to the ion fluxes (J_{anions},$J_{cations}$) that arrive at the electrodes coming from the glass. Usually, in actual experiments the DL width is very small compared to the glass thickness ($\Gamma \ll L$). In those situations, we expect the time variation of the electric field near the cathode to be negligible and then the external current balances up the cation (sodium) flux. That will be confirmed by the numerical simulations described later.

Exclusive Sodium Displacement (The Albaugh Model)

The solution of Eq. 1-12 is straightforward if sodium cations are the only mobile species. We refer to this simple case as the Albaugh model,[6] and we reproduce that solution briefly here because it is a good basis for further improvement and as a reference for the numerical solution which comes later. Analysis of the Albaugh solution also provides the basic motivation for our detailed simulation of the ionic transport.

If only sodium cations are mobile, the charge density within the DL is uniform and local values for the electric field are readily obtainable from Eq. 5 and 6. At the DL front Γ, we have

$$E_\Gamma = \frac{V_0}{L} - \frac{\rho_0}{2\bar{\varepsilon}L}\Gamma^2 \qquad [15]$$

where $\bar{\varepsilon}$ is a mean value for the dielectric constant (which, for simplicity, we assume has the same value for the neutral and for the sodium-depleted glass). The electric field E_Γ decreases to zero from the initial value V_0/L, and Γ reaches its maximum (equilibrium) value at

$$\ell_D = \sqrt{\frac{2\bar{\varepsilon}V_0}{\rho_0}} \qquad [16]$$

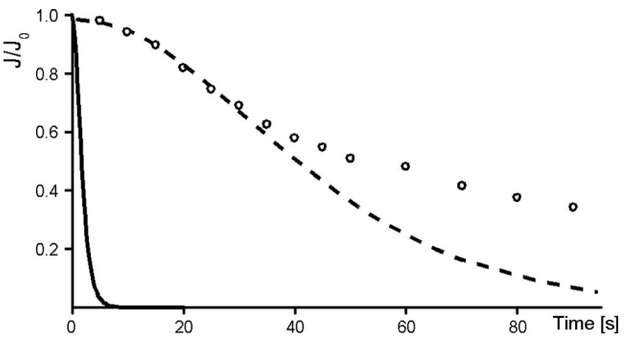

Figure 3. Open circles are the Albaugh experimental points, while the solid curve is Eq. 22 computed with Table I data. The dashed curve is Eq. 22 scaled 22.5 in time.

The electric field at the silicon–glass interface, $E(0)$, increases from the initial value V_0/L to a maximum equilibrium value (when $\Gamma = \ell_D$) given by

$$E(0)^M = \sqrt{\frac{2\rho_0 V_0}{\bar{\varepsilon}}} \qquad [17]$$

Within the ohmic model, Eq. 2, 3, and 15 give a differential equation for the DL front position $\Gamma(t)$

$$\frac{d\Gamma}{dt} = \frac{\mu_{Na^+}V_0}{L}\left(1 - \frac{\Gamma^2}{\ell_D^2}\right) \qquad [18]$$

with analytical solution

$$\Gamma(t) = \ell_D \tanh(t/\tau) \qquad [19]$$

The characteristic time τ is defined as

$$\tau = \frac{2\bar{\varepsilon}L}{\sigma_{Na^+}\ell_D} \qquad [20]$$

The external current is given by Eq. 14, 15, and 18

$$J_{ext} = J^L_{Na^+}(1 - \Gamma/L) \qquad [21]$$

where the sodium flux at the cathode $J^L_{Na^+}$ is equal to the sodium flux at the DL front Γ. As $\Gamma \ll L$ in a typical anodic bonding setup, the external current density equals the cation charge flux at the cathode. Inserting Eq. 19 into Eq. 15 we find, for the external current $i(t)$

$$\frac{i(t)}{I_0} = \mathrm{sech}^2(t/\tau) \qquad [22]$$

where $I_0 = i(0)$. Equation 22 qualitatively matches the observed behavior of the external current decay during anodic bonding setups in which there is uniform Si-g initial mechanical contact. A sigmoid (change in concavity) transition is observed from an initial ohmic behavior to an exponential decay (see Fig. 3). The negative concavity (which mimics an external apparent ohmic behavior, when the electric current is proportional to the external potential) is maintained as long as the rate of increase of the net electric potential drop ΔV_z in the depleted zone is small as compared to the rate of decrease of the potential drop in the bulk (nondepleted) glass. Equation 22 predicts the transition when ΔV_z reaches 33% of the applied external voltage V_0. Available experimental data usually show the sigmoid transition when ΔV_z is between 10 and 20% of V_0.

Equations 18, 19, and 22 were first obtained by Albaugh[6] through a macroscopic equivalent circuit by modeling the DL charge transfer as a charge-dependent capacitor. His predicted characteristic time, which employed the static capacitance of the DL, was higher than Eq. 20 only by a factor of $2^{1/2}$. Equations 19 and 22 were also obtained from a microscopic transport model by Rios et al.[8] and Shih et al.[9]

Table I. Dimensional values of parameters for a typical anodic bonding setup.

	Parameter	Symbol	Value
Experimental settings	Applied voltage	V_0	1000 V
	Glass thickness	L	3.2 mm
Physical properties (Pyrex or Tempax glass)	Dielectric constant	$\bar{\varepsilon}$	$7\varepsilon_0$
	Permittivity of free space	ε_0	8.85×10^{-12} F/m
	Sodium charge content	ρ_0	2.77×10^8 C/m^3
	Ionic resistivity of Na^+	$r = 1/\sigma_{Na^+}$	1.1×10^5 Ω m

Typical glass properties and experimental setups employed for anodic bonding are depicted in Table I. With these values, Eq. 17 predicts that the electric field at the Si-g interface reaches 10^9 V/cm, a value much higher than the rupture field of the glass (around 10^7 V/cm), while Eq. 16 predicts a DL maximum length of around 20 nm (experimental findings strongly support that the DL reaches 1 μm or more). The decaying time, which is around the characteristic time $\tau \cong 2$ s, is also 1–2 orders of magnitude faster than the one which is actually observed.

Those discrepancies show that a charge compensation mechanism must be considered within the DL, allowing redistribution of the negative charge which is left behind as the cations drift toward the cathode. It is apparent that there is no simple remedy which would fit the results of the simple Albaugh model to the experimental findings. For instance, lower values for ρ_0 would increase the equilibrium DL length (Eq. 16) and lower the electric field at the Si-(g) interface (Eq. 17) but at the expense of an even faster transient time (Eq. 20). We also illustrate in Fig. 3 that the long-time behavior of the external current does not follow the exponential decay predicted by Eq. 22. The predictions would work better by employing a high value for effective dielectric constant at the DL, $\bar{\varepsilon}$, something around 10^3. Some authors have suggested that high values of $\bar{\varepsilon}$ can arise due to local space-charge effects.[5] We aim instead at explaining such charge fluctuations by an adequate microscopic transfer model. As pointed out by Wallis, even in the earlier investigations of anodic bonding,[10] the experimental results are more consistent with complete depletion of negative charge in the DL.

A number of useful and improved macroscopic models were developed to mimic the electric transient during anodic bonding by viewing the DL as a charge-dependent lossy capacitor.[5,7] All of the models we are aware of require very high values for the capacitance of the DL. Like the simple Albaugh model, this is achieved by employing very high values for the DL dielectric constant. From the point of view of the more fundamental electrostatic equations, it is obvious from Poisson Eq. 5 that an abnormally high dielectric constant mimics the lack of negative charge in the DL. We thus proceed by considering the effect of displacement of anions while assuming that the dielectric constant is almost the same at the DL and at the bulk glass.

Ionic Processes Within the Depleted Zone

Bonding requires a source of oxygen for oxide formation at the Si-g interface. Therefore, one must consider some other ionic displacement within the depleted zone besides the main sodium flux.

The first possibility is that NBO anions, left behind by the sodium, become mobile and drift toward the anode where they react. While NBO mobility is believed to be very small under ordinary conditions, it may have a role within the high-field region which develops inside most of the sodium-depleted zone.

More recent findings[4] strongly suggest that there are no NBOs at all in Pyrex-like glasses, and sodium cations serve for the charge compensation of $[AlO_4]^-$ and $[BO_4]^-$ groups. The bonding is achieved by the action of water in a leached interface near the surface of the glass.[4] The leached layer is around 500 nm, where water dissociation leaves H^+ and $(OH)^-$ ions available inside the DL. While the H^+ mainly replaces the removed Na^+ ions, hydroxide groups become mobile toward the anode, removing a substantial amount of the residual negative charge from the DL and providing enough oxygen for the bonding reaction.

From the point of view of ionic transport effects, the main factors are the amount and spatial distribution of available mobile charge species inside the DL. In the NBO model, a charge density $-\rho_-$ of O_2^-, or O^- anions[5] becomes available for redistribution in the sodium-depleted region. That "free" anion charge is released at the DL front and it exactly neutralizes the sodium density there (that is, as the DL front Γ advances Δx it releases an amount $-\rho_0 \cdot \Delta x$ of anion charge toward the anode). The NBO source of anions exactly matches the initial sodium content of the bulk glass. The only unknown quantity is μ_-, the NBO mobility in the DL (the zero-mobility case yields the Albaugh equations).

The leached-layer (LL) picture would involve the displacement of both OH^- and H^+ ions. Additional assumptions must be made about the initial composition of the LL, as well as how those ions behave both inside the DL and in the bulk glass. Concentration depth profiles of hydrogen near the metal–glass interface during the bonding process were measured by Nitzsche et al. by the ERDA technique.[4] Measurements in an untreated TEMPAX glass sample indicate that the water content in the LL reaches a maximum around a depth of 200 nm, decreasing continuously thereafter. From their report we can infer that (*i*) the LL depth is around 500–800 nm, where (*ii*) the local hydrogen density (sum of OH^- and H^+ contributions) is at most two times greater than the sodium density, and (*iii*) hydrogen redistribution takes place only inside the depleted sodium zone. We adopt a simplified picture for the ionic transport within the DL in the LL model, which is justified by those measurements: initial uniform densities $-\rho_-^0$ of OH^- and ρ_+^0 of H^+ are assumed, and those ions are only mobile inside the DL. In addition, the LL width is supposed to be large enough to supply dissociated water during the whole transient relevant for the bonding process, which occurs during the first couple of minutes.

Computer Simulations

Both the NBO and the LL charge-transport pictures are investigated here by solving numerically the complete set of Eq. 1-12. The simulation scheme closely follows the physical process that occurs during the time evolution of the DL. Because the DL front speed decreases in time, the calculations are done with a fixed value of a time step Δt. At the ith time interval, the front Γ advances an amount $\Delta^i x$, which becomes progressively smaller in time. The final algorithm is described qualitatively by the following:

1. At each time step Δt, the front displacement $\Delta^i x$ is obtained from a simple discretization of Eq. 2, where the sodium flux at the DL front Γ is computed from by Eq. 3.

2. The space interval $\Delta^i x$ has now mobile charge densities of anions and cations that were left behind by the sodium displacement. These charges have initial values ρ_-^0 and ρ_+^0 and move according to the continuity equations, Eq. 7 and 8 with local fluxes given by Eq. 9 and 10. Updated values for the electric field must satisfy the Poisson Eq. 5 and the total potential drop, Eq. 6. To compute the final charge distribution after the new time step Δt, these sets of

strong coupled nonlinear equations is solved by an iterative, self-consistent technique to ensure numerical stability and reduced rounding errors.

We now briefly give some technical details about the actual numerical implementation. Those readers who are not interested in the numerical details should proceed to the next section.

At the end of the Nth time step, the discrete spatial domain contains $(N + 1)$ nodes x_i (with $x_0 = 0$ and $x_{N+1} = \Gamma$), enclosing N intervals, each one labeled $\Delta^i x$. The electric field and the local fluxes are specified at node locations x_i, and the charge distributions by their mean values within each mesh interval $\Delta^i x$. Because the scheme is based on a fixed value for the time step Δt, a nonuniform spatial mesh is generated by the sodium displacement. Finite differences for Eq. 6 and 7 are written in an implicit form to assure numerical stability. The local fluxes are computed from the arithmetic mean between old and new values for the electric field (a Crank–Nicholson like technique) to improve the numerical truncation error. The charge density at the nodes is computed as a simple arithmetic mean between the neighbor interval mean values.

Because the current mesh interval $\Delta^i x$ decreases in time, we save central processing unit (CPU) time and RAM memory through renormalization of the spatial mesh after a suitable number of time steps. Two adjacent intervals are merged when the charge field gradient is smaller than a given threshold. Thus, as time proceeds, regions where the charge distribution is nearly uniform are solved by coarse meshes.

Our numerical experiments indicated that the anion charge profile $\rho_-(x,t)$ within the DL quickly attains a nearly translation-invariant regime, which remains as long as the front Γ is far away from 0 and L. Therefore, a "traveling wave" guess

$$\rho_-(x,t + \Delta t) = \rho_-(x - \Delta x,t) \qquad [23]$$

is used to achieve faster convergence when solving iteratively the set of Eq. 2-8. This simple strategy allows reduction in CPU times by a factor of 10–100, particularly for large values of the anion mobility μ_-.

The iterated scheme for the numerical integration is detailed as follows:

1. $(i = 0)$ Initial state:uniform electric field $E(x,t) = E_0 = V_0/L$ over a neutral uniform glass $(\rho = 0)$. The DL front is at $\Gamma = 0$.

2. $(i = i + 1)$ Obtain the sodium flux from the current local value of the electric field at Γ (Eq. 3) and then the front dislocation $\Delta^i x$ during the time step Δt (Eq. 2). Increase the DL front location Γ by $\Delta^i x$.

3. Initial charge densities ρ_-^0 and ρ_+^0 are released within $\Delta^i x$ by the sodium displacement. Set $E(x,t + \Delta t) = E(x,t)$ to start the numerical iteration.

4. The final charge distributions ρ_- and ρ_+ are first guessed by Eq. 23; go to step 6.

5. The continuity equations (Eq. 7 and 8) are solved for the charge densities ρ_+ and ρ_- in the domain $0 < x < \Gamma$; in discretized form, this amounts to a tridiagonal system of i algebraic equations. The local fluxes are computed from the arithmetic mean between old and new values of the electric field.

6. The local net charge ρ is updated (Eq. 4), and then corrected values for the local electric field, $E(x,t + \Delta t)$, are obtained according to Eq. 5 and 6.

7. Steps 5 and 6 are iterated; on convergence, renormalize the mesh and go to step 2 until the desired final time is achieved.

Numerical convergence is tested both for the electric field and charge density values. All numerical results are checked for consistency and yield the correct limits when the mobility of cations and anions in the depleted zone approach zero (the Albaugh model). Also, tests for convergence are done by reducing the time step Δt in otherwise identical simulations. Typical runs were done in a 3.5 GHz INTEL-HT PC using a DJGPP C compiler, taking from a few seconds to a couple of hours of CPU time. The CPU time increases dramatically as the mobility of charges in the depletion zone approaches that of the sodium cations (when the various charge transports become strongly coupled).

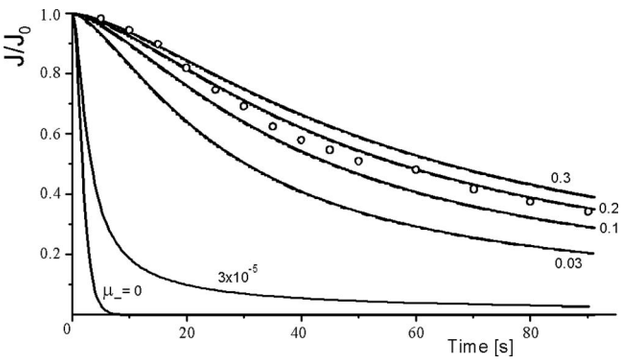

Figure 4. Decay of the normalized electric current in time as a function of the normalized anion mobility (taking the sodium mobility = 1.0). Open circles are experimental points measured by Albaugh.[6] Solid curves are results of the numerical simulations.

Inclusion of Anion Drift (NBO Model)

O_2^- (or O^-) anions of initial density $\rho_-^0 = -\rho_0$ are released at the DL front by the sodium displacement, and those are the only mobile charges within the depleted zone. The unknown parameter is the uncompensated-NBO mobility μ_-.

Numerical simulations with material, electric, and geometric parameters given in Table I led to the results depicted in Fig. 4-6. Those results are essentially the same as some preliminary results previously released by the authors.[11]

The computer simulations correctly reproduce the curves for $\mu_- = 0$, which correspond to the simple Albaugh model. The numerical predictions fit well to the experimental findings when the anion mobility is between 0.1 and 0.3. For $\mu_- = 0.2$, after 1 min of bonding the numerical simulation predicts a sodium depletion width around 450 nm, while the electric field at the Si-g interface reaches $1.6–1.9 \times 10^7$ V/cm (just near above the rupture field of the neutral glass) and the external electric current decays to near 50% of the initial value.

The external electric current is computed from Eq. 14 and is numerically indistinguishable from the cation flux at all times. The anion flux quickly balances the cation flux even for low mobility values, as shown in Fig. 7.

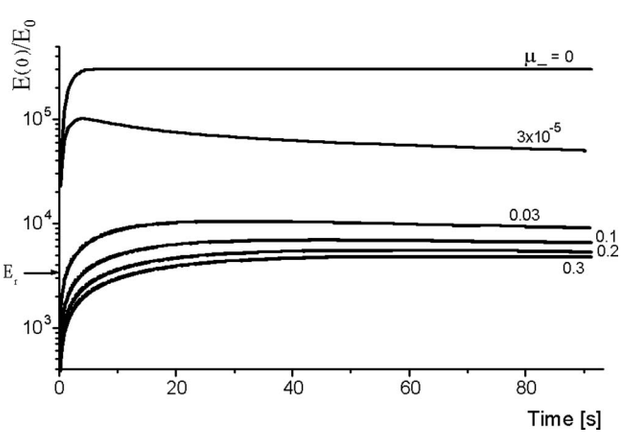

Figure 5. Numerical results for the electric field at the Si-g interface during the anodic transient as a function of the anion mobility. E_r is the rupture field for Pyrex glass.

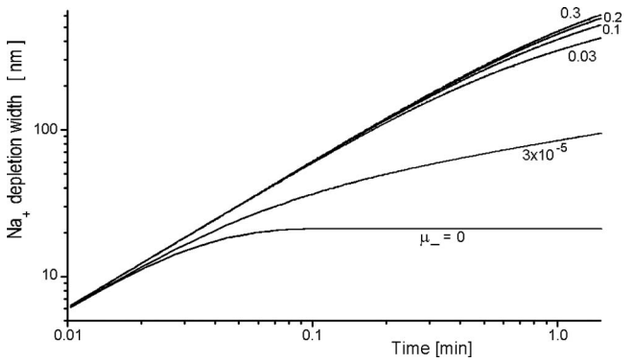

Figure 6. The computed DL width in time as a function of the anion mobility.

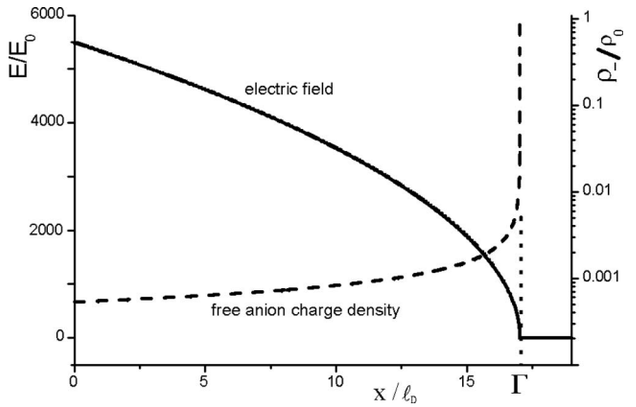

Figure 8. Electric field and anion charge density in the DL for $\mu_- = 0.2$, at time 21.4τ (44.1 s). The total anion charge is $\rho_T = \int_0^\Gamma \rho_-(\xi)d\xi = 0.018\rho_0$.

The anion distribution within the DL quickly attains a nearly steady profile with most of the charge being removed from the high field region, as depicted in Fig. 8. Figure 9 shows that the anion charge is distributed rather evenly through the DL, but the strong nonlinearity discourages attempts to consider more simplified models to circumvent the use of numerical solutions. We actually tried to replace the actual $\rho_-(x,t)$ distribution by a mean value $\bar{\rho}_-(t)$, which would give a linear profile for the integrated charge at the DL, but the results were rather poor. The DL does not behave like a simple lossy charge-dependent capacitor.

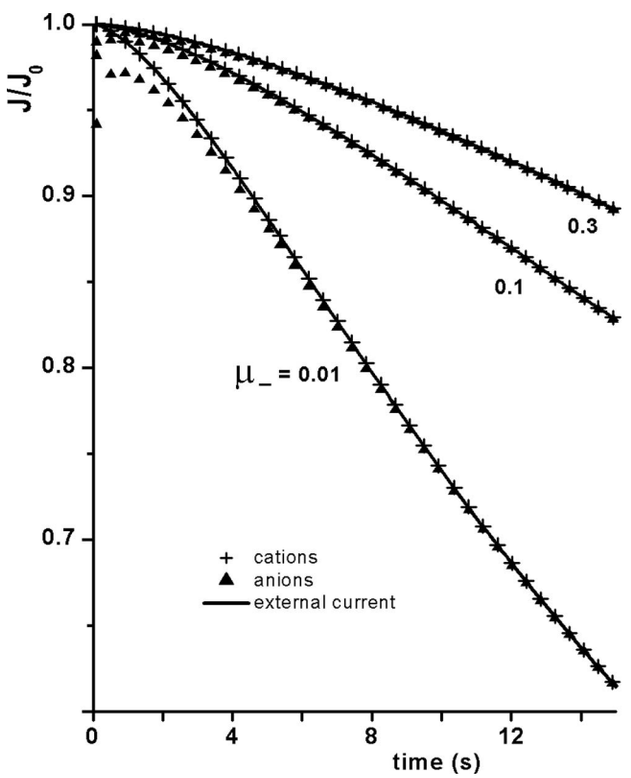

Figure 7. The computed values of J_{ext}, $J_{cations}$, and J_{anions}. Those are the electric fluxes at the electrodes, according to Eq. 14. J_{ext} matches the cation flux at all times.

Mixed Hydroxide Anion and Hydrogen Cation Drift (LL Model)

We now consider that an initial profile of dissociated water in the surface LL is the source of mobile ions within the sodium-depleted zone. That would introduce at least three unknown parameters in the model, namely, initial charge densities $-\rho_-^0 = \rho_+^0$ coming from the dissociated water in the LL, and their mobilities μ_-, μ_+. We argue that the initial charge densities of mobile hydroxide anions OH^-, $-\rho_-^0$, and of the mobile protonic cations H^+, ρ_+^0, cannot be significantly different from the initial sodium content in the glass, ρ_0. To see this, it should be kept in mind that in the LL model, the advance of Na^+ toward the cathode leaves behind a negative immobile background, while mobile anions OH^- drift toward the glass–metal interface; the residual negative charge in the depleted zone must be compensated in part by the redistribution of H^+ there.

"In situ" measurements by Nitzsche et al.[4] show that redistribution of hydrogen occurs only inside the DL, toward the cathode, leaving a growing hydrogen-depleted layer near the Si-g interface. Thus, a deficit of OH^-–H^+ mobile pairs as compared to the initial sodium content ($-\rho_-^0 < \rho_0$) would cause a static layer of background uncompensated negative charge to develop quickly near the metal–glass interface, dramatically hampering the advance of the depletion front. That is confirmed by our numeric simulations. The effect of a small (0.3%) deficit of mobile OH^-–H^+ pairs on the

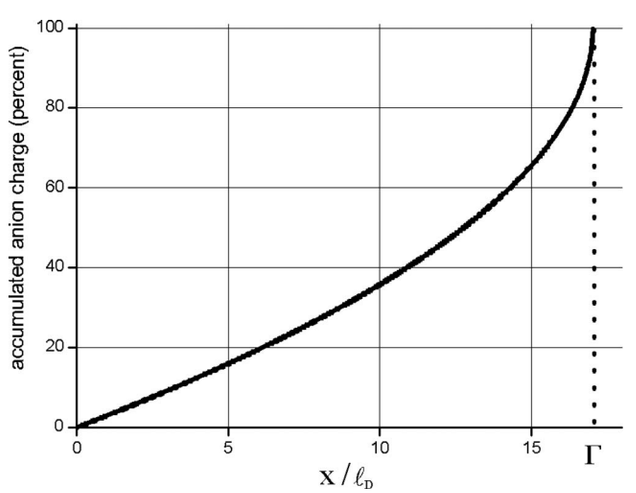

Figure 9. Integrated anion charge profile $\int_0^x \rho_-(\xi)d\xi$ in the DL, corresponding to Fig. 8, as a fraction of ρ_T.

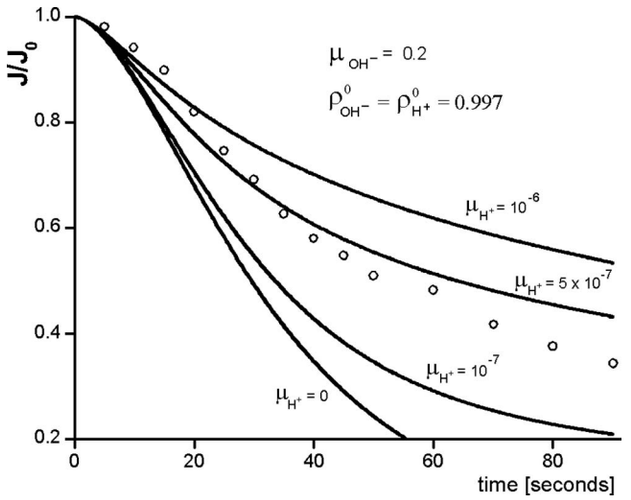

Figure 10. Computed external current decay when the initial concentration of mobile OH^-–H^+ pairs is 0.3% less than sodium cations in the depleted zone. Open circles are the Albaugh experimental points.

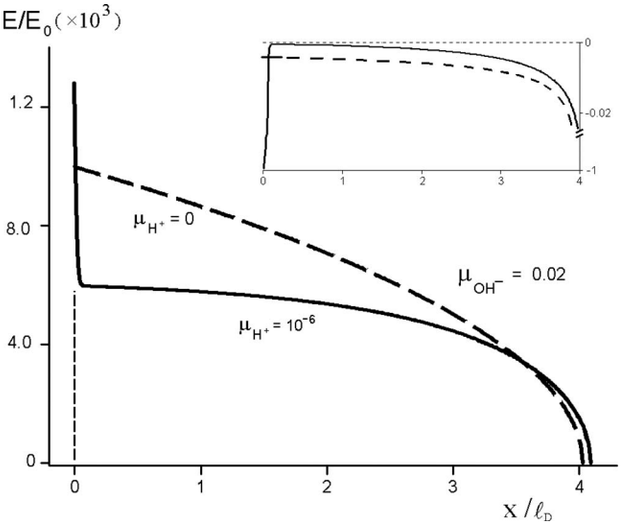

Figure 12. Effect of H^+ transport on the electric field profile inside the depleted zone. The field at the Si-g interface gets higher but flattens at the bulk, resulting in a net 25% less potential drop; as a result, the depletion front advances faster. The graphs are for OH^- mobility 0.02 after 9.0 s of bonding. The inset shows the total charge distribution inside the DL.

external current behavior is depicted in Fig. 10. The calculations were done for $\mu_{OH^-} = 0.2$ and should be compared to Fig. 4, which shows the computed external current for $-\rho_-^0 = \rho_0$ and $\mu_+ = 0$. It is also apparent that the decay in the external current is very sensitive to H^+ redistribution inside the DL.

The observed behavior of the external current decay and of the depleted zone length rules out the possibility of positively charged regions within the sodium depleted zone. Therefore, because hydrogen redistribution occurs only inside the DL,[4] from where the OH^- anions are continuously removed and consumed at the anode, only a small excess of OH^-–H^+ mobile pairs as compared to the initial sodium content ($-\rho_-^0 > \rho_0$) would be conceivable. In that case, our simulations show that the external current decay does not agree well to the experimental measurements (Fig. 11).

H^+ redistribution in the depleted zone causes the Na depletion front to advance faster, while slowing down the external current decay. In contrast, enhancing the Na mobility would speed up both the depletion front and the current decay. It is apparent that the advancement of the depleted zone can be made appreciable even for low anion mobility; high residual negative charges are compensated by redistribution of the hydrogen cations. This effect is illustrated in Fig. 12. Redistribution of H^+ lowers the net charge density and flattens the electric field in the bulk of the depleted zone, thus reducing the potential drop ΔV_z. As a result, the DL front advances faster, but at the expense of increasing the electric field in the Si-g interface (which will become depleted of any mobile ions). This kind of hydrogen redistribution matches qualitatively the long-time measurements done by Nitzsche et al.[4]

Increasing either the initial density of mobile OH^-–H^+ pairs or the hydrogen mobility in the depleted zone also brings the sigmoid transition to early times. This, as should become apparent from Fig. 10 and 11, does not lead to a detailed accurate description of the external current decay. Figure 13 shows that an almost perfect fitting

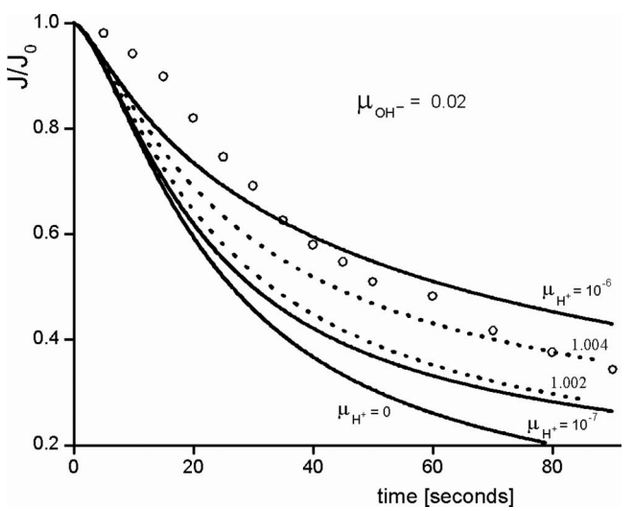

Figure 11. Solid curves are for $\rho^0_{OH^-} = \rho^0_{H^+} = 1.000 = \rho^0$. Dashed curves are for hydrogen cation mobility = 10^{-8}, and increasing values of OH^-–H^+ initial concentration.

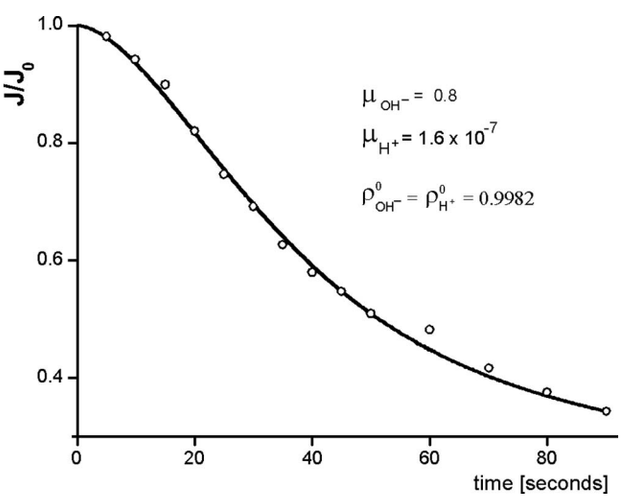

Figure 13. The external electric current transient is reproduced by the numerical simulations for high anion mobility in the DL, along with very low hydrogen mobility and a very small deficit of OH^-–H^+ pairs in the LL, relative to the initial sodium content in the glass.

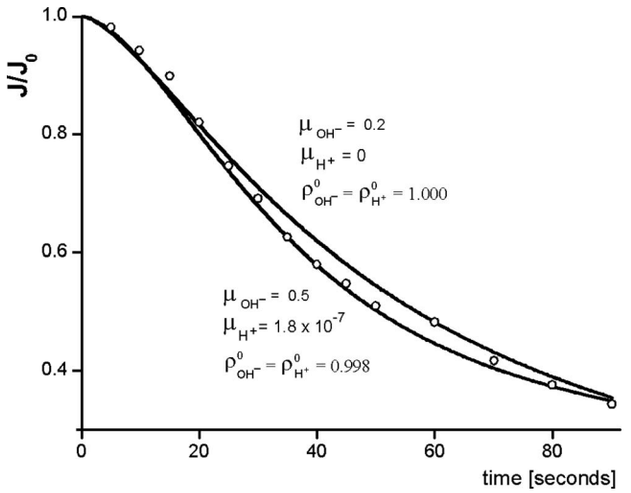

Figure 14. Good fittings are also obtained for parameters similar to the optimum values.

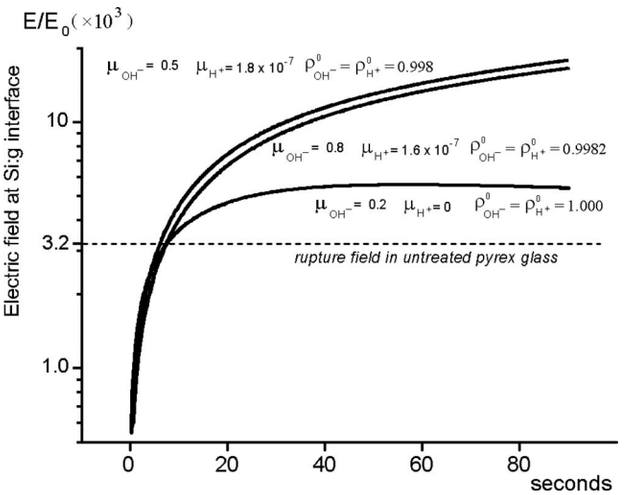

Figure 16. The predicted local electric field at the Si-g interface becomes very high due to the cumulative effects of the hydrogen drift and the deficit of free carriers in the DL.

can be achieved assuming (*i*) very high hydroxide anion mobility, (*ii*) a small deficit on the initial mobile OH^-–H^+ composition as compared to the sodium content, and (*iii*) very small hydrogen cation mobility. Because Albaugh reported that a good mechanical Si-g contact was already established in the first 15 s of bonding,[6] we treat the sigmoid transition which shows up in his experimental data as a relevant feature of the ionic transport in the DL. The numerical values depicted in Fig. 13 are not to be taken strictly, because the current decay behavior is very sensitive to small differences in the initial charge profile within the LL. Also, we show in Fig. 14-16 that similar results can be obtained by distinct values (though qualitatively in the same range) of the parameters. This range of H^+ and OH^- mobilities and concentrations is therefore the only one available for fitting the experimental current data to the LL model. Comparison with independently obtained mobility data for OH^- in borosilicate glasses is not possible, however. Data on the separate contribution of different ions to conduction in borosilicate glasses is not available, even though there is mention of significant contribution of OH^- in silicate glasses and in sodium metaphosphate.[12,13] Possibly the best source for these independent measurements would be bonded glass samples themselves because the sodium depletion is already well established.

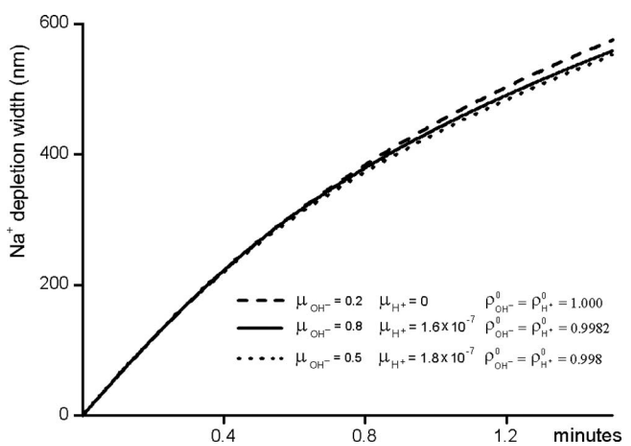

Figure 15. The DL width, as predicted by the numerical simulations, is almost the same for the three sets of parameter values employed in Fig. 13 and 14. A mere 0.2% deficit of H^+–OH^- pairs compensates for the influence of larger mobility values.

If OH^-–H^+ transport is the correct relevant process during bonding, there must be some compensating effect for the high increase of the electric field in the vicinity of the Si-g interface caused by the resulting frozen negative background. Possibly, these high values would be reduced by the potential drop across the growing oxide layer in the bonding region (which we did not consider here). Hydrogen redistribution may also be hindered at later times in the low-field region of the depleted zone. Deviations from the ohmic transport model adopted here would be certainly expected. Also, network modifiers at the "frozen" background, such as $[AlO_4]^-$ and $[BO_4]^-$, could in some way migrate to the anodic bonding region or behave in an unexpected manner under a very high electric field.

It is intriguing that only concentrations of OH^- and H^+ mobile ions very close (within 0.2%) to the sodium concentration lead to the correct behavior of the external current decay. Remarkably enough, the measurements of Nitzsche et al.[4] of the hydrogen content in a untreated sample of Tempax (Schott 8330) glass show a diffusion-limited LL around 800 nm thickness, with a peak value near the glass free-surface; the peak concentration is indeed two hydrogen atoms per sodium atom, that is, one H^+ and one OH^- per sodium atom. In the presence of a strong enough external electric field, Na^+ cations and OH^- anions become mobile, and the unpaired hydrogen cations slowly redistribute over the DL, showing very low mobility under the external electric field.

Conclusions

We have shown that the observed external electric transient behavior during bonding can be explained by a detailed microscopic charge-transfer model, taking into account the main few ionic species which have so far been experimentally detected. Although working with some simplified assumptions, such as a general linear ohmic behavior, the simulation helps in understanding the role of charge redistribution within the sodium-depleted layer. They also show that the slow decay of the electric transient at longer times is due to the continuous release of charge carriers at the sodium-depleted front and their subsequent removal by the strong local electric field. Thus, the persistency of the bonding current at longer times is accounted for by considering the presence of anions with appreciable mobility inside the DL.

Two distinct models were investigated concerning the origin of ionic mobile species. The NBO model assumes that nonpaired O^- becomes mobile in the high field region which arises by the sodium

cation drift. If NBO is absent, the relevant mobile ionic species in the sodium-depleted zone are OH^- and H^+, originating from water dissociation in a LL near the glass surface. Our results show that both models compare well to the observed behavior of the external electric current transient, charge distribution, and time evolution of the sodium-depleted layer. More recent and detailed charge measurements[4] favor the LL model as the actual ionic process during anodic bonding. In that case, our charge-transfer simulations show that the observed decay time of the process is only explained for very low hydrogen mobility, along with an almost perfect balance between the density of free carriers and the sodium content in the glass. As mentioned previously, the measurements of Nitzsche et al.[4] are consistent with that. One is left with the task of understanding why water would be absorbed exactly in such a one-to-one ratio to sodium. Somehow, water absorption in the glass seems to be limited by its sodium content.

The numerical treatment allows consideration of more detailed and accurate models. For instance, (*i*) deviations from a pure ohmic transport are expected for the dissociated ionic species within the DL; (*ii*) the actual detailed ionic composition profile in the glass LL is likely to have some impact in the decay time and external current behavior predicted by the numerical simulations; (*iii*) there is an additional potential drop caused by the oxide layer formation at the Si-g interface; (*iv*) the effect of sodium deposition near the cathode; and (*v*) other mobile ionic species present in the glass could have been considered.

A more attractive possibility is to investigate the long-time behavior of the external electric current. The hydrogen transport and the DL width have already been measured in situ by Nitzsche et al.[4] on a time scale of hours. That was not carried out here because a quantitative comparison with experimental results would require a detailed study of the initial charge distributions in a number of nontreated glass samples. Besides, long-time decay is not directly relevant to practical anodic bonding and may require consideration of carrier diffusion as well.

References

1. G. Wallis and D. I. Pomerantz, *J. Appl. Phys.*, **40**, 3946 (1969).
2. A. T. J. van Helvoort, K. M. Knowles, R. Holmestad, and J. A. Fernie, *Philos. Mag.*, **84**, 505 (2004).
3. D. E. Carlson, K. W. Hang, and F. Stockdale, *J. Am. Ceram. Soc.*, **55**, 337 (1972).
4. P. Nitzsche, K. Lange, B. Schmidt, S. Grigull, U. Kreissig, B. Thomas, and K. Herzog, *J. Electrochem. Soc.*, **145**, 1755 (1998).
5. K. M. Knowles and A. T. J. van Helvoort, *Int. Mater. Rev.*, **51**, 273 (2006).
6. K. B. Albaugh, *J. Electrochem. Soc.*, **138**, 3089 (1991).
7. K. M. Knowles, *Adv. Sci. Technol. (Faenza, Italy)*, **45**, 1558 (2006).
8. A. N. Rios, A. C. Gracias, I. A. Maia, and J. R. Senna, *Rev. Bras. Aplic. Vacuo*, **19**, 31 (2000).
9. W.-P. Shih, C.-Y. Hui, and N. C. Tien, *J. Appl. Phys.*, **95**, 2800 (2004).
10. G. Wallis, *J. Am. Ceram. Soc.*, **53**, 563 (1970).
11. M. Fabbri and J. R. Senna, in *XXV CILAMCE, Iberian Latin America Congress on Computational Methods in Engineering*, Recife, Brazil (CD-ROM, ISBN 8574098698) (2004): also available at http://www.las.inpe.br/~fabbri/Fabbri&Senna_cilamce_2004a.pdf.
12. W. Muller and K. Forkel, *Z. Chem.*, **22**, 45 (1982), as cited by H. Scholze, *Glass, Nature, Structure and Properties*, p. 303, Springer-Verlag, New York (1991).
13. V. N. Naraev, K. K. Evstrop'ev, and A. A. Pronkin, *Sov. J. Glass Phys. Chem.*, **9**, 70 (1983), as cited by H. Scholze, *Glass, Nature, Structure and Properties*, p. 303, Springer-Verlag, New York (1991).